Journal of Power Sources 196 (2011) 4573–4578

Contents lists available at ScienceDirect

Journal of Power Sources

journal homepage: www.elsevier.com/locate/jpowsour

Performance degradation of direct formic acid fuel cell incorporating a Pd anode catalyst

Won Suk Jung, Jonghee Han*, Sung Pil Yoon, Suk Woo Nam, Tae-Hoon Lim, Seong-Ahn Hong

Fuel Cell Research Center, Korea Institute of Science and Technology, 39-1 Hawolgok-dong, Seongbuk-gu, Seoul 136-791, Republic of Korea

ARTICLE INFO

Article history:
Received 18 August 2009
Received in revised form 2 October 2009
Accepted 12 November 2009
Available online 26 November 2009

Keywords:
Direct formic acid fuel cell
Palladium catalyst
Performance degradation
Surface poisoning
Particle size growth

ABSTRACT

Electrochemical and physical analysis is employed to verify the performance degradation mechanism in direct formic acid fuel cells (DFAFCs). The power density of a single cell measured at 200 mA cm^{-2} decreases by 40% after 11 h of operation. The performance of the single cell is partly recovered however, by a reactivation process. Various analytical methods such as scanning electron microscopy (SEM), transmission electron microscopy (TEM), and electrochemical impedance spectroscopy (EIS) are used to investigate the mechanism of performance degradation. The analytical results show that the electrolyte membranes in the DFAFC are stable for 11 h of operation after the reactivation process. The major factors causing performance degradation in the DFAFC are an increment in the anode charge-transfer resistance and a growth in the particle size of the Pd anode catalyst. The anode charge-transfer resistance, confirmed by EIS, increases with operation time and is due to poisoning of the catalyst surface. Although it is not clear what chemical species poisons the catalyst surface, the catalyst surface is cleaned by the reactivation process. Performance losses caused by surface poisoning are completely recovered by the reactivation process. Increase in catalyst size induces a reduction in active surface area, and the performance loss caused by the growth in catalyst size cannot be recovered by the reactivation process.

1. Introduction

Direct liquid fuel cells (DLFCs) are considered a promising candidate to replace batteries in portable electronics such as cell-phones, portable multimedia players, and laptop computers. Among the different types of DLFCs, direct methanol fuel cells (DMFCs) have received the most attention over many years [1–3]. Nevertheless, direct methanol fuel cells are still under development due to drawbacks that include slow kinetics, methanol cross-over, and toxicity. Each of these drawbacks must be overcome to commercialize DMFCs. For these reasons, some researchers have tried to find alternative fuels for DLFCs, namely, formic acid [4–7], ethanol [8–10], and propanol [11,12]. Among them, formic acid has attracted particular interest due to its many advantages as an alternative fuel. Formic acid is a liquid at room temperature and is safe when in dilute form [13,14]. The cross-over flux of formic acid through Nafion® is lower than that of methanol [15], and this enables the use of thinner membranes and the utilization of concentrated formic acid solution as a fuel. Also, low cross-over flux decreases the loss in cell performance caused by the mixed electrode potential.

Electro-oxidation of formic acid on a catalyst is faster than that of methanol because formic acid has a very simple molecular structure and its theoretical electromotive force (emf) is higher than that of methanol. These intrinsic characteristics of formic acid permit operation of direct formic acid fuel cells (DFAFCs) at a power density about 3–6 times greater than that of DMFCs at room temperature [5].

Since the components of DFAFCs are the same as those of DMFCs, except for the anode catalyst, many researchers have focused on the development of anode catalysts for DFAFCs. In general, DFAFCs use anode catalysts based on precious metals such as Pt and Pd. Many workers have investigated Pt black [7] and Pt-bimetallic catalysts (e.g., PtRu [16,17], PtAu [18–20], PtPb [21–23], and PtBi [24,25]). Ha et al. [5,26] have demonstrated that a Pd-based anode is highly active for the electro-oxidation of formic acid and that single cells with a Pd catalyst give a maximum power density of 240 mW cm^{-2} at a current density of 600 mA cm^{-2}. Since then, Pd black and Pd-bimetallic catalysts such as PdIr [27], PdV [28], PdSn [29] and PdCo [30] have been studied intensively. In most cases, however, the Pd-based catalysts deactivated rapidly with operation time. Although the rapid deactivation of the Pd-based catalysts in DFAFCs caused serious performance deterioration, the performance could be recovered to previous levels by applying an anodic potential (1.0 vs. a dynamic hydrogen electrode) to the anode [5,31,32]. These observations suggest that deactivation of the Pd-based catalysts in

* Corresponding author. Tel.: +82 2 958 5277; fax: +82 2 958 5199.
E-mail address: jhan@kist.re.kr (J. Han).

0378-7753/$ – see front matter © 2011 Published by Elsevier B.V.
doi:10.1016/j.jpowsour.2009.11.085

DFAFCs might be caused by poisoning of their surfaces, but the exact deactivation mechanism has still to be elucidated. In this study, an attempt is made to identify the deactivation mechanism by operation of a single cell and application of various electrochemical and physical analyses.

2. Experimental

2.1. MEA preparation and single-cell operation

Membrane–electrode assemblies (MEA) were fabricated in-house by means of direct paint technique as described in elsewhere [5–7]. The active area of the electrode was 9 cm^2. The catalyst inks were prepared by dispersing catalyst powders in appropriate amounts of Millipore water and 5 wt.% recast Nafion® solution (1100 EW, Sigma–Aldrich). The catalyst inks for the anode and cathode were painted directly on both sides of a Nafion® 115 membrane. Pt black (HiSPEC™ 1000 from Johnson Matthey) was used as the cathode catalyst layer at a loading of 7 mg cm^{-2}. Pd black (High Surface Area from Sigma–Aldrich) was used as the anode catalyst at a loading of 8 mg cm^{-2}. The final anodic and cathodic catalyst layers contained 10 and 15 wt.% Nafion®, respectively.

The cell polarization of the prepared MEA was measured by a galvanostatic method using an electric loader (EZPD, ESL-300Z) at 30 °C. An aqueous solution of 5 M formic acid was fed into the anode at a constant flow rate of 5 ml min^{-1}, while dry air was supplied to the cathode at a flow rate of 800 sccm. Continuous operation of the single cell was carried out at a constant current density of 200 mA cm^{-2}. To recover deactivated MEAs, a reactivation process was conducted. In the reactivation process, H_2 was introduced at the cathode side, while 5 M formic acid was supplied to the anode side. The H_2/Pt in the cathode side acts as dynamic hydrogen electrode (DHE). In this study, a potential of 1.1 V vs. DHE was applied to the anode of the deactivated DFAFC for 3 s. The details of this procedure have been presented in elsewhere [5,31].

2.2. Electrochemical and physical analysis

Electrochemical impedance spectroscopy and cyclic voltammetry were carried out to characterize the electrochemical properties of the prepared MEAs. A coupled frequency response analyzer (Solartron 1260) and potentiostat (Solartron 1286) controlled by a computer were used for electrochemical analysis. For the analysis, 5 M formic acid and deionized water were fed to the anode at a flow rate of 5 ml min^{-1}. To use the cathode as a counter electrode as well as a DHE, hydrogen gas was supplied to the cathode at a flow rate of 400 sccm.

Impedance spectra were measured between 1 kHz and 1 Hz with 10 steps per decade at 30 °C. The amplitude of the sinusoidal potential signal was fixed at 10 mV. To avoid inductance along the electrical cable, the length of the cables was minimized and the cables were not in tangled. Cyclic voltammetry (CV) was performed at a scan rate of 20 mV s^{-1} by sweeping potential between 0 and 1.2 V (vs. DHE) at 30 °C. Before the measurements, deionized water was fed to the anode (the working electrode) for at least 20 min in order to remove any remaining formic acid from the catalyst surface.

Various physical techniques were used to observe the morphology of the Pd catalysts. At various points during operation, MEAs were examined by SEM (FEI XL-30 FEG) and TEM (Philips STEM CM-30).

3. Results and discussion

3.1. Performance degradation and reactivation

The cell polarization and power density plots measured while using 5 M formic acid solution and dry air at 30 °C are presented in Fig. 1. Initially, the cell displayed high performance and the maximum power density was 187 mW cm^{-2} at 556 mA cm^{-2}. The cell performance drastically decreases (as reported in the literature [31–33]), and the maximum power density measured after 11 h of operation is 76 mW cm^{-2} at 200 mA cm^{-2}, which represents only 40% of the initial value. As shown in Fig. 1, the cell performance could be recovered by a simple reactivation process that applies an anode potential of 1.1 V (vs. DHE) for 3 s. After reactivation process, the cell performance is recovered immediately and the maximum power density returns to a value of 136 mW cm^{-2} at 333 mA cm^{-2}. When surface poisoning of the anode catalyst is the only major reason for performance degradation, the performance of the cell should be recovered to its initial value after a reactivation process that cleans the surface of the anode catalyst. In this case, however, the cell performance did not fully recover to its initial value; the maximum power density after the reactivation process is about 73% of its initial value. This implies that the degradation in cell performance involves one or more mechanisms other than surface poisoning of the anode catalyst. To identify the mechanism of performance degradation in a DFAFC with the Pd-based anode, a variety of characterization methods were employed; the results are presented below.

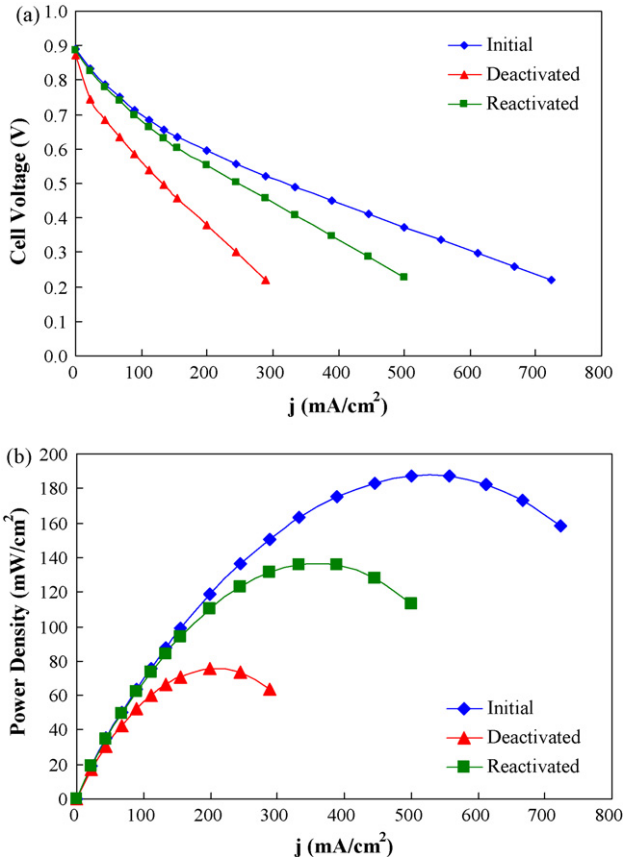

Fig. 1. Single cell (a) polarization and (b) power density plots at initial, deactivated and reactivated steps. 5 M formic acid and dry air without back pressure fed to anode and cathode at flow rates of 5 ml min^{-1} and 800 sccm, respectively, at 30 °C.

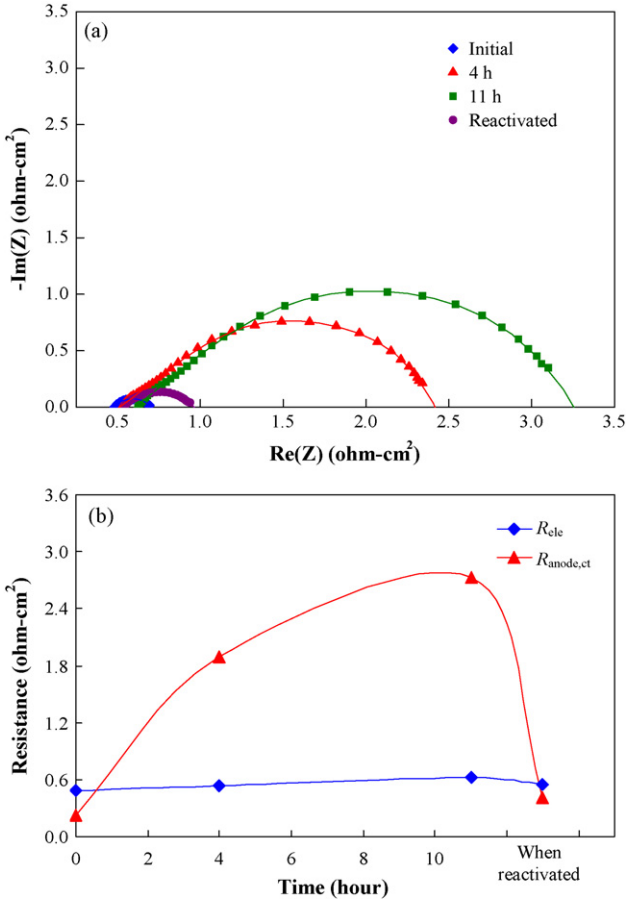

Fig. 2. (a) EIS (Nyquist plots) of Pd-based anode in DFAFCs as function of operation time at ambient temperature. (b) Values of R_{ele} and $R_{anode,ct}$ at various cell operation times are extracted from (a). 5 M formic acid fed to anode at a flow rate of 5 ml min^{-1}. H_2 at 400 sccm supplied to cathode so that this electrode serves as both counter electrode and dynamic hydrogen electrode.

3.2. Effect of electrolyte on performance degradation

The first characterization method employed to verify the performance degradation mechanism was the a.c. impedance analysis. Fig. 2 shows the Nyquist plots of the DFAFC single-cell measured at 30 °C during three different stages: the initial stage of the operation (before performance degradation), the operation after degradation (11 h operation at constant current density of 200 mA cm^{-2}), and operation after a reactivation process. The electrolyte resistance (R_{ele}) and anode charge-transfer resistance ($R_{anode,ct}$) values as a function of the cell operation time were extracted from Fig. 2(a); herein the electrolyte resistance indicates the ohmic resistance because the electrical resistance of the electrolyte is much larger than that of the other components in polymer electrolyte-based fuel cells. The diameter of the semi-circle shown in Fig. 2, which represents the charge-transfer resistance, was obtained by extrapolating the last points in the low frequency region on to the *x*-axis.

As shown in Fig. 2(a), the value of the R_{ele} is almost constant during the 11 h operation. There is little change in the R_{ele} value, even if the cell was reactivated. This constant internal resistance implies that the performance of the electrolyte is stable during this experiment. These results are consistent with our previous results [32].

To observe physical distortion of the electrolyte membrane, SEM analysis was performed on the cross-section of each MEA. The micrographs of MEAs in three different stages namely, the initial stage, after degradation from 11 h of operation, and after the reactivation process, are presented in Fig. 3. To avoid deformation of the fractured cross-section during preparation, each sample was broken after immersion in liquid nitrogen. Due to the compression pressure of the cell, all of the membranes are thinner than their thickness before the experiment (i.e., 95–100 μm vs. 127 μm). As shown in Fig. 3, however, the thickness of each sample is in a similar range, with a difference of only 5 μm at most. Consequently, the electrolyte membrane is considered to be stable during the

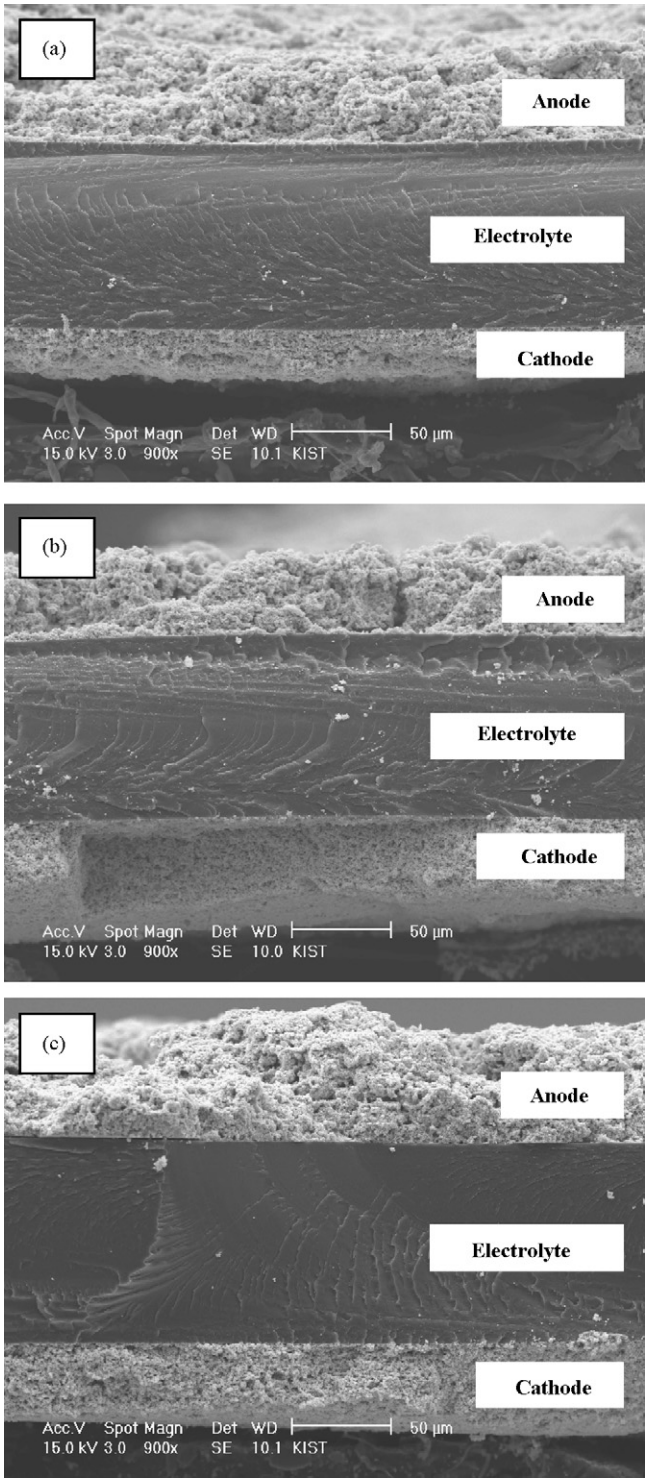

Fig. 3. Cross-sectional SEM images of Pd-based catalyst layers: (a) initial surface, (b) deactivated anode, and (c) reactivated anode. All images measured with 900 magnification.

operation time, and the electrolyte membrane is not considered to be a major cause for the performance degradation.

3.3. Electrochemical analysis on anode

As shown in Fig. 2(a), the impedance spectra taken at the initial stage and after the reactivation process appear to consist of a single semi-circle. By contrast, impedance spectra taken after 4 and 11 h of operation seem to consist of two semi-circles. Reports in the literature indicate that distortion of the semi-circles in a Nyquist plot is caused by surface poisoning [34]. Also the $R_{anode,ct}$ increases continuously with operation time. The value of the $R_{anode,ct}$ after a reactivation process is 0.407 ohm-cm^2, whereas the values after 0, 4, and 11 h of operation are 0.23, 1.9 and 2.7 ohm-cm^2, respectively. Here 0 h of operation time refers to the initial stage of the cell operation. These date indicate that the $R_{anode,ct}$ increases while the single cell is being operated continuously for 11 h. In a previous study [32], we reported that the $R_{anode,ct}$ increases as a function of the operation time when the impedance spectra are measured while applying a constant overpotential to the anode. Also, it was found that the $R_{anode,ct}$ decreases after the reactivation process. These observations are similar to the results of the present study. The $R_{anode,ct}$ increases by a factor of twelve during the operation time, and both the $R_{anode,ct}$ and the cell performance are easily recovered by the reactivation process. As mentioned above, however, the cell performance and $R_{anode,ct}$ are not recovered to their initial values. Considering the synchronized behaviour of $R_{anode,ct}$ and cell performance, it is clear that the performance degradation is mainly caused by the anode overpotential.

In order to characterize the anode polarization in detail, CV was carried out between 0.6 and 1.2 V (vs. DHE) at 30 °C. The first scans taken at initial stage, after 11 h of operation and after the reactivation process are presented in Fig. 4. Two peaks at 0.92 and 1.09 V appear in the case of the Pd-based anode after 11 h of operation. Several research groups have reported that the two distinct peaks correspond to the desorption of CO_{ads} or unknown species on the Pd surface at 0.9 and 1.1 V (vs. DHE), respectively [32,35]. These poisoning materials immediately vanish during the reactivation process, as shown in Fig. 4.

From the impedance spectra and CV measurements given in Figs. 2 and 4, the anode degradation caused by surface poisoning of the Pd catalyst can be easily recovered, although these poisoning materials negatively influence DFAFC performance.

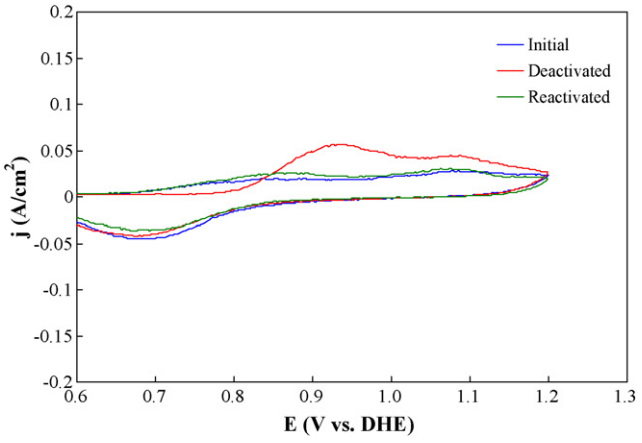

Fig. 4. CV diagrams for initial, deactivated and reactivated Pd-based anode in DFAFCs. CV diagrams consist of first scan between 0.6 and 1.2 V (vs. DHE). Deionized water and H_2 without back pressure fed to anode and cathode at flow rates of 5 ml min^{-1} and 800 sccm, respectively, at 30 °C. Scan rate 20 mV s^{-1}.

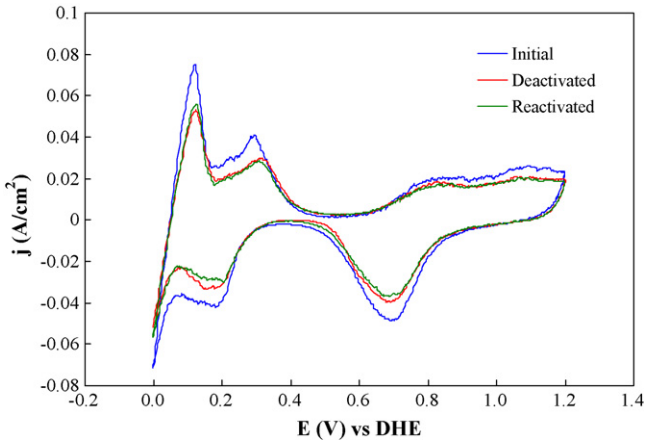

Fig. 5. CV diagrams for initial, deactivated and reactivated Pd-based anode in DFAFCs. CV diagrams consist of fourth scan between 0 and 1.2 V (vs. DHE). Deionized water and H_2 without back pressure fed to anode and cathode at flow rates of 5 ml min^{-1} and 800 sccm, respectively, at 30 °C. Scan rate 20 mV s^{-1}.

3.4. Characterization of physical properties of anode

The CV plots of MEAs in the initial stage, after 11 h of operation, and after the reactivation process are shown in Fig. 5. To avoid explosion, nitrogen was fed to the cathode for at least 20 min before the measurement. The CV experiments were carried out between 0 and 1.2 V (vs. DHE) at 30 °C. Deionized water and dry hydrogen were supplied to the anode and the cathode, respectively.

In general, the area of the hydrogen desorption peak (between 0.11 and 0.28 V) is not used to estimate the electrochemically active surface area (ECASA) of the Pd-based anode because of the hydrogen absorption ability of Pd [36]. Nevertheless, the ECASA of the Pd catalyst was estimated from the area of the hydrogen desorption peaks appearing in the CV diagram. To validate this ECASA estimation method, the effect of hydrogen absorption was minimized by several methods. First of all, the amount of Pd catalysts loaded on the anodes was fixed and identical pretreatment procedures were applied before the CV tests. This ensures that the amount of absorbed hydrogen in the anodes to remains at the same level. Also, deionized water was introduced into the anode side instead of an acid solution. This minimizes both hydrogen evolution and the hydrogen source for absorption.

If it is assumed that the ECASA of the initial Pd-based anode is 100% with respect to the hydrogen desorption plot, then the ECASAs for the Pd-based anodes of the MEAs after 11 h of operation and after the reactivation process are about 75 and 72%, respectively.

In many cases, the ECASA reduction is caused by the aggregation of the catalyst particles. The aggregation of the catalyst particles makes the particle size grow and it reduces the surface area of the catalyst particles. To examine the growth in the particle size, TEM analysis was performed. From the TEM images of catalysts taken from the MEAs at different stages, it is clearly observed that the particle sizes of the Pd catalyst after 11 h of operation and after the reactivation process are both larger than those of the initial MEA. To quantify the particle size of the Pd catalyst, the sizes of the catalyst particles from the TEM images, and the size distributions of catalyst particles from each MEA are presented in Fig. 6. The most frequent particle size of the Pd catalyst from the initial MEA is about 5–7 nm. On the other hand, the most frequently appearing particle sizes of catalysts from the deactivated and the reactivated MEAs are each about 8–10 nm. It is clear that the particle size of the Pd catalyst grows with operation. Furthermore, the reactivation process does bit exert any influence on the particle size of the Pd catalyst.

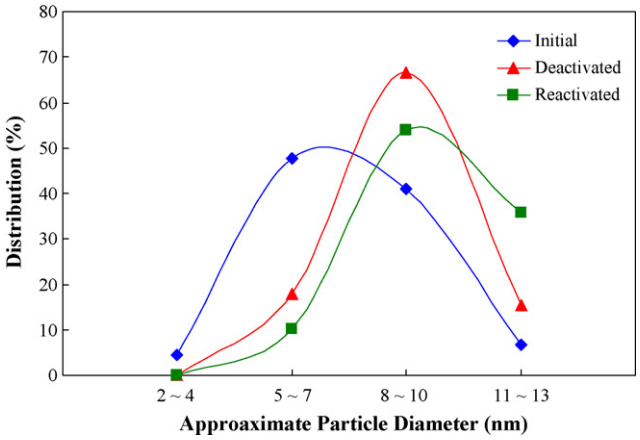

Fig. 6. Grain size distribution diagrams of Pd in initial, deactivated and reactivated steps.

In summary, deactivation of the Pd catalyst is caused by two different mechanisms: surface poisoning of the Pd catalyst and aggregation of the catalyst particles. The reactivation process can recover cell performance that has been deactivated by surface poisoning, but the performance degradation caused by particle aggregation cannot be recovered. This means that aggregation between the catalyst particles is a serious problem over the life of the DFAFCs.

In order to investigate the long-term stability of cell performance, as well as the catalyst particle size, the same cycle that was used in the 11-h operation experiment was repeated. First, the CV and cell polarization were measured before operation. Then the cell was galvanostatically operated at a constant 200 mA cm^{-2} for 11 h. After this service, the deactivated MEA was reactivated and the cell polarization was measured. This process was repeated four consecutive times. The fifth CV scan of the MEA is given in Fig. 7(a) and the change in ECASA and power density at 200 mA cm^{-2} measured after the reactivation process is presented in Fig. 7(b). As mentioned before, the reactivation process cleans the surface of the catalyst, and the power density measured after the reactivation process includes the power density loss from the aggregation only. This means that the power loss caused by surface poisoning is excluded by the reactivation process. The initial values of ECASA and power density at 200 mA cm^{-2} are taken as 100% in Fig. 7(b). As shown in Fig. 7, the amounts of adsorption and desorption of hydrogen and oxygen are diminished as the operation proceeds. The ECASA decreases rapidly in the first and second cycles (22 h total operation time). After the third cycle, the ECASA obtained from the curve for hydrogen desorption is not significantly altered. In each cycle, the ECASA decreases by approximately 35% compared with the initial ECASA. The power density trend is similar to that of ECASA, are shown in Fig. 7(b). The power density decreases rapidly during the first and the second cycle. After the second cycle, the power densities become stable. Consequently, the long-term stability test shows that the aggregation between the catalyst particles occurs in the first two cycles (22 h of operation), and that reduction in ECASA causes performance degradation. After the second cycle, the rate of ECASA reduction and performance degradation becomes slower so that the two parameters achieve stability. To confirm the aggregation effect of the catalyst particles, the Pd catalyst from a MEA operated for 44 h (four cycles) was analyzed by TEM; an image is shown in Fig. 8. The degree of aggregation after 44 h MEA is more severe than that in a MEA after 11 h. There is no doubt that the Pd catalyst particles have aggregated and that the ECASA has been reduced. Based on the presentations in Figs. 7 and 8, it is clear that the cell performance is degraded because of the loss in ECASA caused by particle size growth [37].

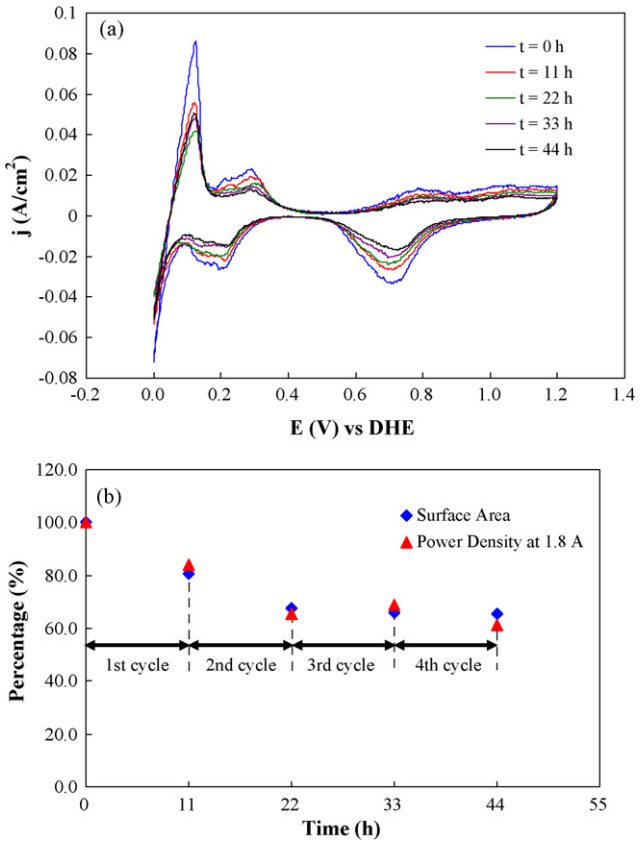

Fig. 7. (a) CV diagrams of Pd-based anode as function of operation time in DFAFC. CV diagrams consist of fourth scan at each time. Deionized water and H_2 without back pressure fed to anode and cathode at flow rates of 5 ml min^{-1} and 400 sccm, respectively, at 30 °C. Scan rate 20 mV s^{-1}. (b) Decrease in power density at 200 mA cm^{-2} and ECASA of Pd-based anode as function of operation time at 30 °C. 5 M formic acid and dry air without back pressure fed to anode and cathode at flow rates of 5 ml min^{-1} and 800 sccm, respectively.

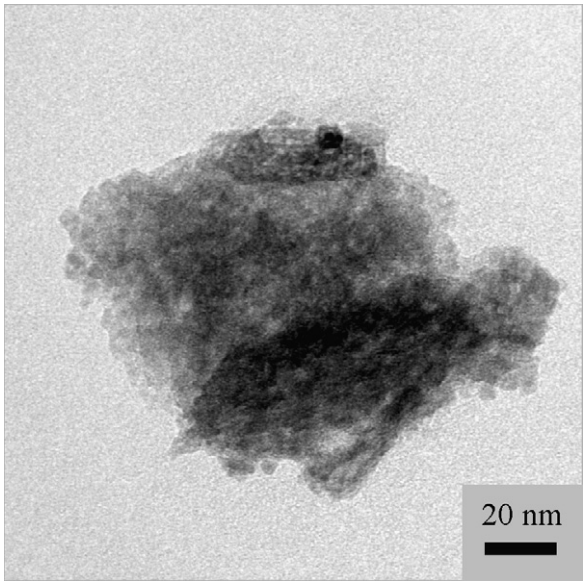

Fig. 8. TEM image of deactivated Pd particles for 44 h.

4. Conclusion

The mechanism of performance degradation in the anode of DFAFCs has been investigated by physical and electrochemical analyses. Whereas the electrolyte membrane is stable during cell operation, degradation of the Pd-based anode occurs through two mechanisms: (i) poisoning of the electrode surface and (ii) the aggregation of catalyst particles. The performance is only partially recovered by a reactivation process. The unrecovered performance is caused by aggregation of the catalyst particles. The rate of aggregation for the initial 22 h is faster than that during 22–44 h of operation. The change in power is also due to the aggregation of catalyst particles. The aggregation is unaffected by the reactivation process.

Acknowledgement

This work was supported by the Korea Institute of Science and Technology.

References

[1] A. Blum, T. Duvdevani, M. Philosoph, N. Rudoy, E. Peled, Journal of Power Sources 117 (2003) 22–25.
[2] H. Chang, J.R. Kim, J.H. Cho, H.K. Kim, K.H. Choi, Solid State Ionics 148 (2002) 601–606.
[3] X. Ren, P. Zelenay, S. Thomas, J. Davey, S. Gottesfeld, Journal of Power Sources 86 (2000) 111–116.
[4] S. Ha, B. Adams, R.I. Masel, Journal of Power Sources 128 (2004) 119–124.
[5] S. Ha, R. Larsen, Y. Zhu, R.I. Masel, Fuel Cells 4 (2004) 337–343.
[6] C. Rice, S. Ha, R.I. Masel, P. Waszczuk, A. Wieckowski, T. Barnard, Journal of Power Sources 111 (2002) 83–89.
[7] C. Rice, S. Ha, R.I. Masel, A. Wieckowski, Journal of Power Sources 115 (2003) 229–235.
[8] C. Lamy, S. Rousseau, E.M. Belgsir, C. Coutanceau, J.M. Leger, Electrochimica Acta 49 (2004) 3901–3908.
[9] F. Vigier, C. Coutanceau, A. Perrard, E.M. Belgsir, C. Lamy, Journal of Applied Electrochemistry 34 (2004) 439–446.
[10] W. Zhou, Z. Zhou, S. Song, W. Li, G. Sun, P. Tsiakaras, Q. Xin, Applied Catalysis B: Environmental 46 (2003) 273–285.
[11] D. Cao, S.H. Bergens, Journal of Power Sources 124 (2003) 12–17.
[12] Z. Qi, M. Hollett, A. Attia, A. Kaufman, Electrochemical and Solid-State Letters 5 (2002) A129–A130.
[13] US Code of Federal Regulations, 21 CFR 186.1316.
[14] US Code of Federal Regulations, 21 CFR 172.515.
[15] Y.-W. Rhee, S.Y. Ha, R.I. Masel, Journal of Power Sources 117 (2003) 35–38.
[16] C.M. Miesse, W.S. Jung, K.-J. Jeong, J.K. Lee, J. Lee, J. Han, S.P. Yoon, S.W. Nam, T.-H. Lim, S.-A. Hong, Journal of Power Sources 162 (2006) 532–540.
[17] N.M. Markovic, H.A. Gasteiger, P.N. Ross, X. Jiang, I. Villegas, M.J. Weaver, Electrochimica Acta 40 (1995) 91–98.
[18] J.K. Lee, J. Lee, J. Han, T.-H. Lim, Y.-E. Sung, Y. Tak, Electrochimica Acta 53 (2008) 3474–3478.
[19] J.B. Xu, T.S. Zhao, Z.X. Liang, Journal of Power Sources 185 (2008) 857–861.
[20] Z. Peng, H. Yang, Nano Research 2 (2009) 406–415.
[21] S. Uhm, S.T. Chung, J. Lee, Electrochemistry Communications 9 (2007) 2027–2031.
[22] L.J. Zhang, Z.Y. Wang, D.G. Xia, Journal of Alloys and Compounds 426 (2006) 268–271.
[23] F. Matsumoto, C. Roychowdhury, F.J. DiSalvo, H.D. Abruña, Journal of the Electrochemical Society 155 (2008) B148–B154.
[24] M.D. Maci, E. Herrero, J.M. Feliu, Journal of Electroanalytical Chemistry 554–555 (2003) 25–34.
[25] S. Uhm, H.J. Lee, Y. Kwon, J. Lee, Angewandte Chemie International Edition 47 (2008) 10163–10166.
[26] S. Ha, Z. Dunbar, R.I. Masel, Journal of Power Sources 158 (2006) 129–136.
[27] X. Wang, Y. Tang, Y. Gao, T. Lu, Journal of Power Sources 175 (2008) 784–788.
[28] R. Larsen, J. Zakzeski, R.I. Masel, Electrochemical and Solid-State Letters 8 (2005) A291–A293.
[29] Z. Liu, X. Zhang, Electrochemistry Communications 11 (2009) 1667–1670.
[30] X. Wang, Y. Xia, Electrochemistry Communications 10 (2008) 1644–1646.
[31] S. Ha, R. Larsen, R.I. Masel, Journal of Power Sources 144 (2005) 28–34.
[32] W.S. Jung, J. Han, S. Ha, Journal of Power Sources 173 (2007) 53–59.
[33] R. Larsen, S. Ha, J. Zakzeski, R.I. Masel, Journal of Power Sources 157 (2006) 78–84.
[34] D.A. Blom, J.R. Dunlap, T.A. Nolan, L.F. Allard, Journal of the Electrochemical Society 150 (2003) A414–A418.
[35] Y. Zhu, Z. Khan, R.I. Masel, Journal of Power Sources 139 (2005) 15–20.
[36] M. Łukaszewski, K. Kuśmierczyk, J. Kotowski, H. Siwek, A. Czerwiński, Journal of Solid State Electrochemistry 7 (2003) 69–76.
[37] H. Kim, S.-J. Shin, Y.-g. Park, J. Song, H.-T. Kim, Journal of Power Sources 160 (2006) 440–445.